Bull. Mater. Sci., Vol. 32, No. 3, June 2009, pp. 361–367. © Indian Academy of Sciences.

Structure, synthesis and multiferroic nature of $BiFeO_3$ and $0{\cdot}9BiFeO_3$–$0{\cdot}1BaTiO_3$: An overview

DHANANJAI PANDEY* and ANAR SINGH

School of Materials Science and Technology, Institute of Technology, Banaras Hindu University, Varanasi 221 005, India

Abstract. **A brief review of the crystal structure and multiferroic nature of pure $BiFeO_3$ and $0{\cdot}9BiFeO_3$–$0{\cdot}1BaTiO_3$ (BF–0·1BT) is presented. An atomic level evidence for magnetoelectric coupling of intrinsic multiferroic origin in BF–0·1BT is presented.**

Keywords. **Multiferroics; magnetoelectrics; $BiFeO_3$.**

1. Introduction

Materials exhibiting spontaneous polarization, magnetization and deformation, whose direction can be reversed by an external electric field, magnetic field and stress are termed as ferroelectric, ferromagnetic and ferroelastic, respectively. The antiferroelectric and antiferromagnetic materials are also regarded as ferroics, although they could have been termed as antiferroics as well. Materials in which atleast two of the three ferroic orders coexist are called multiferroics. Recent years have witnessed resurgence of interest in magnetoelectric multiferroics in which ferroelectric and magnetic orders not only coexist in the same material but also couple with each other such that the magnetic degree of freedom can be manipulated by an electric field and *vice versa* (Fiebig 2005; Eerenstein *et al* 2006; Ramesh and Spaldin 2007; Cheong and Mostovoy 2007; Rao and Serrao 2007). The magnetoelectric coupling (ME) in multiferroics promises important technological applications in several multifunctional devices like data storage, spinotronics, sensor and actuator devices, etc (Fiebig 2005; Ramesh and Spaldin 2007). The coexistence of ferroelectric and magnetic orders offers interesting challenges for condensed matter theorists too. It has been shown that ferroelectricity in ABO_3 perovskites originating from off-centring of B-site transition metal cations (such as Ti^{4+} in $BaTiO_3$) requires empty d orbitals (d^0 electrons) for the hybridization of 3d Ti and 2p O orbitals. Further, the development of ferroelectric order requires breaking of the spatial inversion symmetry. Magnetism, on the contrary, requires transition metal ions with partially filled d orbitals (d^n electrons) and the breaking of the time reversal symmetry. The two phenomenon, which thus appear to be mutually exclusive, have nevertheless been found to coexist in a small number of magnetoelectric multiferroics which should exhibit asymmetry in space and time both.

The coexistence of ferroelectric and magnetic orders has been found in compounds where the origin of ferroelectricity does not lie in the 'd^0-ness' of the transition metal ion going off-centre in the ferroelectric state. For example, compounds like $BiMnO_3$ or $BiFeO_3$ with magnetic Mn^{3+} and Fe^{3+} ions, it is the Bi ion with $6s^2$ lone pair electrons that moves away from the centrosymmetric position in its oxygen surroundings leading to ferroelectricity (Hill 2000). There are other multiferroic compounds, where ferroelectricity appears as an accidental byproduct of spiral magnetic ordering (Cheong and Mostovoy 2007), charge ordering (Brink and Khomskii 2008) or geometrical distortion in the framework structure (Aken *et al* 2004).

$BiFeO_3$ is unique amongst various magnetoelectric multiferroics, as its ferroelectric and magnetic transition temperatures are well above the room temperature. This raises the possibility of developing potential devices based on magnetoelectric coupling operating at the room temperature. As a result, $BiFeO_3$ has received tremendous attention over the last few decades and the last couple of years have witnessed several new results on this compound in pure and solid solution forms. In this article, we briefly review the structure and multiferroic characteristics of pure $BiFeO_3$ and present an overview of our results on magnetoelectric coupling of intrinsic multiferroic origin in solid solutions of $BiFeO_3$ with $BaTiO_3$, published recently (Singh *et al* 2008).

2. Structure and multiferroic character of $BiFeO_3$

Bulk $BiFeO_3$ has got a rhombohedrally distorted perovskite structure in the $R3c$ space group with $a^-a^-a^-$ tilt system (Glazer 1972) in which the neighbouring oxygen

*Author for correspondence (dpandey_bhu@yahoo.co.in)

octahedra of the elementary perovskite cell are rotated anti-clockwise about the [111] direction due to a ferroelastic transition involving R (q = 1/21/21/2) point phonon (Jacobson and Fender 1975). In this distorted structure, the hexagonal $[001]_h$ is equivalent to the pseudo-cubic $[111]_c$ direction, which is the three fold rotation axis of the $R3c$ space group. Both Bi^{3+} and Fe^{3+} cations are displaced from their centrosymmetric positions in the room temperature phase giving rise to permanent dipole moment required for ferroelectric order. There are three atoms in the asymmetric unit of $BiFeO_3$ occupying the following Wyckoff positions: 6a (Bi^{3+} and Fe^{3+}) and 18b (O^{2-}). The Rietveld analysis using neutron scattering has shown Z_{Bi} = 0·2987, Z_{Fe} = 0·0196, X_O = 0·2379, Y_O = 0·3506 (Fischer *et al* 1980). The tilt angle for antiphase rotation of the oxygen octahedra at room temperature is found to be ω = 12·2° (Fischer *et al* 1980). The Fe magnetic moments are coupled ferromagnetically within the pseudocubic (111) planes and antiferromagnetically between adjacent planes leading to the so called G-type antiferromagnetic ordering. The G-type antiferromagnetic ordering in $BiFeO_3$ is better visualized in the elementary perovskite cell. The magnetic ordering is not spatially homogeneous but rather a spatially incommensurate modulated in a spin spiral structure with an approximate periodicity of 620 Å. The spins in this spiral structure gradually rotate on the $(110)_h$ plane while the modulation wave vector is $[110]_h$ (Sosnowska *et al* 1982). This long period spiral modulated magnetic structure leads to the cancellation of the net macroscopic magnetization over the periodicity of the spin spiral. This is responsible for the near absence of linear magnetoelectric effect (Popov *et al* 1993; Eerenstein *et al* 2006).

Until recently, it has not been possible to prepare highly insulating single crystalline or ceramic samples of $BiFeO_3$, and as a result it was not possible to measure their ferroelectric polarization. However, in recent years, good quality single crystals of pure $BiFeO_3$ with high insulating resistance have been grown (Lebeugle *et al* 2007). Measurements on such crystals have revealed extremely high polarization close to 100 μC/cm^2 and nearly linear M–H response (Lebeugle *et al* 2007). Using single crystals, it has been shown that the ferroelectric/ferroelastic domains of $BiFeO_3$ can be switched from one orientation variant to another by an external electric field (Lebeugle *et al* 2008; Lee *et al* 2008b). But what is more interesting from the point of view of magnetoelectric coupling in this multiferroic is that the wave vector of the spin spiral also switches on switching the ferroelectric domains. Magnetoelastic coupling in $BiFeO_3$ has been revealed through the observation of anomalies in the unit cell parameters across the magnetic transition temperature, T_N (Palewicz *et al* 2007).

The incommensurate cycloidal spin structure is reported to be suppressed by the application of a high magnetic field >18 T (Ruette *et al* 2004), chemical substitutions (Wang *et al* 2005) and nanosizing (Mazumder *et al* 2007). Significant magnetization (1 μ_B/unit cell) and linear magnetoelectric effect have been observed in highly insulating epitaxial thin films showing Ps ~ 60 μC/cm^2, suggesting that the spiral spin structure could possibly be suppressed in thin films also (Wang *et al* 2003), even as doubts have been expressed on these results as trace amount of γ-Fe_2O_3 present as an impurity phase, well below the detection limit of X-ray diffraction, may possibly be responsible for the observation of weak ferromagnetism in the thin films (Eerenstein *et al* 2005). A similar observation has been made by Lee *et al* (2008b) in single crystal of $BiFeO_3$.

3. Synthesis and room temperature structure of 0·9$BiFeO_3$–0·1$BaTiO_3$ (BF–0·1BT)

The synthesis of phase pure $BiFeO_3$ powders through solid state route is very difficult due to the formation of a thermodynamically stable impurity phase $Bi_2Fe_4O_9$. It has been reported that this impurity phase can be removed by leaching the powder with dilute nitric acid (Sosnowska *et al* 1982; Kumar and Palkar 2000). However, the fact remains that once $Bi_2Fe_4O_9$ has been formed, the overall stoichiometry of the $BiFeO_3$ phase would be considerably modified in order to maintain the mass balance of starting reagents. This enhances the leakage current and therefore, gives very poor ferroelectric loops. Liquid-phase rapid sintering and rapid annealing of presintered $BiFeO_3$ ceramics have been reported to improve the electrical properties (Wang *et al* 2004; Zhang *et al* 2005). An alternative method for preparing phase pure and insulating samples of $BiFeO_3$ is by forming its solid solution with other ABO_3 perovskites (Wang *et al* 2005; Bhattacharjee *et al* 2007, 2009).

We have prepared phase pure samples of solid solutions of $BiFeO_3$ and $BaTiO_3$ by solid state route. To get rid of the impurity phase $Bi_2Fe_4O_9$, which commonly forms during the synthesis of the $BiFeO_3$ due to easy volatility of Bi_2O_3, we have calcined the powders at lowest possible temperatures. Figure 1 depicts the X-ray diffraction pattern of the solid solution of 0·9$BiFeO_3$–0·1$BaTiO_3$ (BF–0·1BT) calcined at different temperatures 953, 973, 993, 1013 and 1033 K, respectively for 8 h. It is evident from this figure that an impurity phase, identified as $Bi_{36}Fe_2O_{57}$, is formed at 953 K along with the dominant perovskite phase of BF–0·1BT. As the calcinations temperature is increased, the intensity of the impurity peak gradually decreases. When the calcination temperature is increased to 1033 K, the XRD pattern indicates formation of single phase of BF–0·1BT. The monophasic calcined powder was sintered for 1 h at 1173 in closed alumina crucible sealed with MgO powder with calcined powder of the same composition as spacer powder for preventing the loss of Bi_2O_3 during sintering.

The room temperature structure of BF–0·1BT also remains rhombohedral in the *R*3*c* space group similar to pure $BiFeO_3$. This was confirmed by Rietveld refinement. Coordinates of all the atoms in the asymmetric unit cell as a function of the displacement parameters *s*, *t*, *d* and *e*, as per Megaw and Darlington (1975), are: Bi^{3+}/Ba^{2+} (0, 0, 1/4 + *s*), Fe^{3+}/Ti^{4+} (0, 0, *t*), O^{2-} (1/6 –2*e* –2*d*, 1/3 –4*d*, 1/12). The parameters '*s*' and '*t*' describe the polar displacement of cations Bi^{3+}/Ba^{2+} and Fe^{3+}/Ti^{4+} along $[111]_{rh}$ or $[001]_h$. The tilt angle ω is related to the displacement parameter '*e*' of oxygen O^{2-} from its ideal position by the expression $\omega = \tan^{-1}(4e3^{1/2})$ (Megaw and Darlington *et al* 1975) whereas parameter '*d*' is related to the distortion of the BO_6 (B: Fe^{3+}/Ti^{4+}) octahedron parallel to the $[111]_{rh}$ axis. The *z* coordinates of the oxygen atom is fixed in this representation. Figure 2 depicts the Rietveld fits of BF–0·1BT at room temperature using *R*3*c* space group and the refined parameters are listed in table 1. The tilt angle for this composition is ~11·2° which is close to the value of 12·2° for pure $BiFeO_3$.

4. Magnetoelectric coupling in $0{\cdot}9BiFeO_3$–$0{\cdot}1BaTiO_3$ (BF–0·1BT)

Coupling of magnetic and electric order parameters can be studied directly by measuring the change in polarization induced by an external magnetic field or by measuring changes in the magnetization by an applied electric field (Eerenstein *et al* 2006). An alternative way to investigate magnetoelectric coupling is the measurement of magnetocapacitance (Kimura *et al* 2003b). Furthermore, an anomaly in the dielectric constant at the magnetic transition temperature is predicted on the basis of Landau theory in multiferroic materials on account of magnetoelectric coupling (Kimura *et al* 2003a). However, in sintered polycrystalline samples of multiferroic materials, such a dielectric anomaly at the magnetic transition temperature may not necessarily result from multiferroicity of the bulk sample only, as it may also have significant contributions from the interfacial layers (i.e. grain boundaries, grain–electrode interfaces) of different resistivities (Catalan 2006).

Introduction of 10% $BaTiO_3$ in $BiFeO_3$ leads to weak ferromagnetic *M*–*H* hysteresis loop (see inset of figure 3(a)) which may be due to the partial suppression of spiral magnetic order. Our powder neutron scattering studies have revealed that the magnetic structure remains antiferromagnetic, which suggest that the *M*–*H* loop could be due to the canting of the spins. The temperature dependence of the inverse of d.c. magnetic susceptibility (at 500 Oe) is depicted in figure 3(a). This gives the magnetic transition temperature as $T_C \sim 648$ K. The magnetic transition has been confirmed by the heat flow measurements which is also shown in figure 3(a). It shows an anomaly at the magnetic transition temperature. Further, temperature dependence of the real part of the dielectric constant at very high frequencies 500, 700 and 1000 kHz shows a peak at the magnetic transition temperature (see figure 3(b)). At these high frequencies, the contribution of space charge (grain boundary and grain electrode surfaces) is negligible, and only the intrinsic dielectric constant of the grains contributes to the measured value (Singh *et al* 2008). In order to confirm the presence of intrinsic (bulk) as well as the interfacial (space charge) contributions to the measured values of the dielectric constant, we carried out impedance spectroscopic analysis using Cole–Cole plots in the complex Argand plane. In the Cole–Cole plots, the circular arc for the lowest

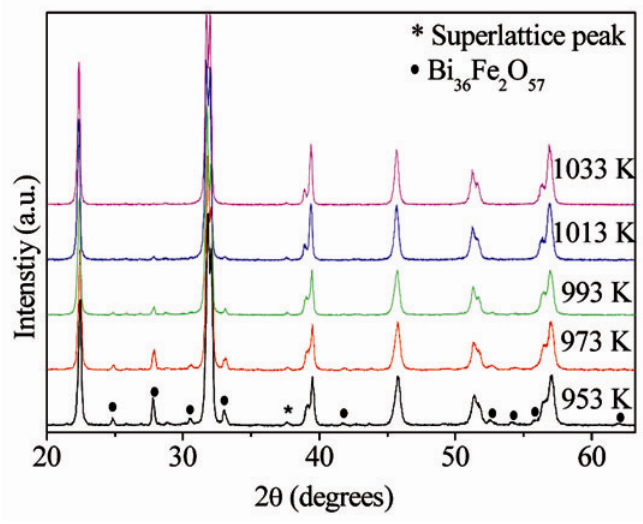

Figure 1. X-ray diffraction patterns of the solid solution $0{\cdot}9BiFeO_3$–$0{\cdot}1BaTiO_3$ (BF–0·1BT) calcined at different temperatures 953, 973, 993, 1013 and 1033 K.

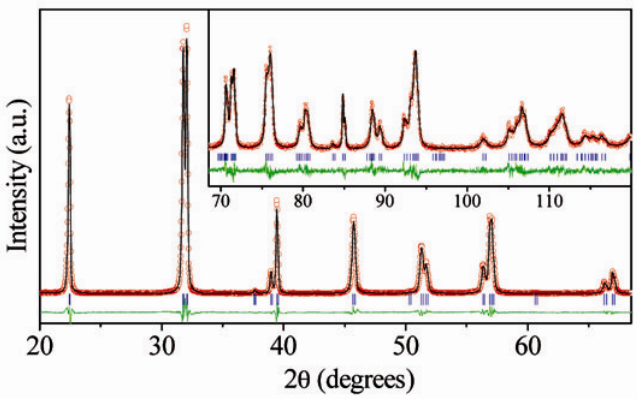

Figure 2. Observed (open circle), calculated (line) and difference (bottom curve) profiles obtained after Rietveld refinement of powder diffraction data of BF–0·1BT in the 2θ range of 20°–120° for rhombohedral *R*3*c* space group. The tick marks above the difference plot show the positions of the Bragg peaks for the rhombohedral *R*3*c* space group.

Table 1. Refined structural parameters of BF–0·1BT at 300 K and $BiFeO_3$ at 293 K (Fischer *et al* 1980) using *R*3*c* space group.

	$BiFeO_3$–0·1$BaTiO_3$				$BiFeO_3$		
	a_h = 5·5854(2) Å, c_h = 13·8674(3) Å β = 120°, $\alpha = \gamma$ = 90°				a_h = 5·585(7) Å, c_h = 13·884(18) Å β = 120°, $\alpha = \gamma$ = 90°		
Ions	*x*	*y*	*z*	B(Å^2)	*x*	*y*	*z*
Bi^{3+}/Ba^{2+}	0	0	0·2971(3)	1·04(2)	0	0	0·2987(5)
Fe^{3+}/Ti^{4+}	0	0	0·0197(4)	0·39(6)	0	0	0·0196(5)
O^{2-}	0·235(2)	0·355(2)	0·0833	0·8(2)	0·2379(8)	0·3506(12)	0·8333

R_p = 7·01, R_{wp} = 9·79, R_{exp} = 6·56 and χ^2 = 2·23

Table 2. Theoretical calculation of basis function of irreducible representation with displacement vectors for the symmetry *R*3*c* with *k* = 0 for the Wyckoff site 6*a*: Bi (0, 0, 1/4 + *s*) and Fe (0, 0, *t*) (after EPAPS Document 2008).

			Site 6*a*	
Irreducible representations	Basis function		(*x*, *y*, *z*)	(–*y*, –*x*, *z* + 1/2)
IR(1)	Basis (1)		(001)	(001)
IR(2)	Basis (1)		(001)	(00 –1)
IR(3)	Basis (1)	Re	(1·50 0·00 0·00)	(0·00 0·00 0·00)
		Im	(–0·87 –1·73 0·00)	(0·00 0·00 0·00)
	Basis (2)	Re	(0·00 1·50 0·00)	(0·00 0·00 0·00)
		Im	(1·73 0·87 0·00)	(0·00 0·00 0·00)
	Basis (3)	Re	(0·00 0·00 0·00)	(0·00 –1·50 0·00)
		Im	(0·00 0·00 0·00)	(–1·73 –0·87 0·00)
	Basis (4)	Re	(0·00 0·00 0·00)	(–1·50 0·00 0·00)
		Im	(0·00 0·00 0·00)	(0·87 1·73 0·00)

frequency range corresponds to the electrode–grain interface, the arc for the intermediate frequency range represents grain boundary contributions and the arc in the high frequency range represents the grain (or bulk) contribution. Figure 4 gives the Cole–Cole plots for the complex impedance ($Z^* = Z' - iZ''$) of BF–0·1BT in the 100 Hz to 1 MHz frequency range at two selected temperatures: 425 and 575 K. The Cole–Cole plots in this figure clearly reveal the presence of three overlapping semicircular arcs at 575 K which may be attributed to contributions from the grain, grain boundary and electrode–grain interfaces in the decreasing order of measuring frequencies. For $T \leq 425$ K, these three polarization processes are not resolved. This is due to the difference in the temperature dependence of relaxation times associated with the three different polarization processes with different activation energies and has been confirmed using impedance spectroscopy analysis. The grain boundary and electrode–grain contributions are insignificant above 400 kHz and hence the dielectric anomaly in figure 3(b) at frequencies ≥ 500 kHz represents the intrinsic magnetoelectric coupling only.

The intrinsic magnetoelectric coupling was further confirmed through detailed crystallographic analysis of high temperature X-ray diffraction data. The unit cell volume (V) and the rhombohedral angle (α) display anomalies at the magnetic transition temperature (see figure 3(c)). These anomalies in V and α suggest strong spin-lattice coupling. Further, the temperature variation of the change in the atomic coordinates (δ) from their ideal positions (Bi/Ba (0, 0, 1/4 ± δz), Fe/Ti (0, 0, ± δz) and O(1/6 ± δx, 1/3 ± δy, 1/12)) also shows significant shift below the magnetic transition temperature. This is depicted in figure 3 (d, e, f and g). The shift in the atomic positions below the magnetic transition temperature were analysed in terms of the possible irreducible representations of the *R*3*c* space group using BasIreps package (Hovestreydt *et al* 1992). The atomic displacement modes calculated for each position of *R*3*c* space group symmetry at *k* = 0 can be decomposed into the following representations for the Wyckoff 6*a* and 18*b* sites: $IR_{6a} = IR(1) + IR(2) + 2IR(3)$, $IR_{18b} = 3IR(1) + 3IR(2) + 6IR(3)$ (see tables 2 and 3). We find that the experimentally observed displacements for BF–0·1BT shown in figure 3 (d, e, f and g) are consistent with the *IR*(1) mode of the group theoretical predictions. The sense of the atomic displacements of *IR*(1) (Basis(1)) mode for Bi/Ba, Fe/Ti and O atoms are shown in figure 5. The fact that the observed shift in the atomic positions below the magnetic transition temperature can be visualized in terms of the *IR*(1) mode of the *R*3*c* space group suggests that there is a structural phase transition accompanying the magnetic transition at 648 K. However, this

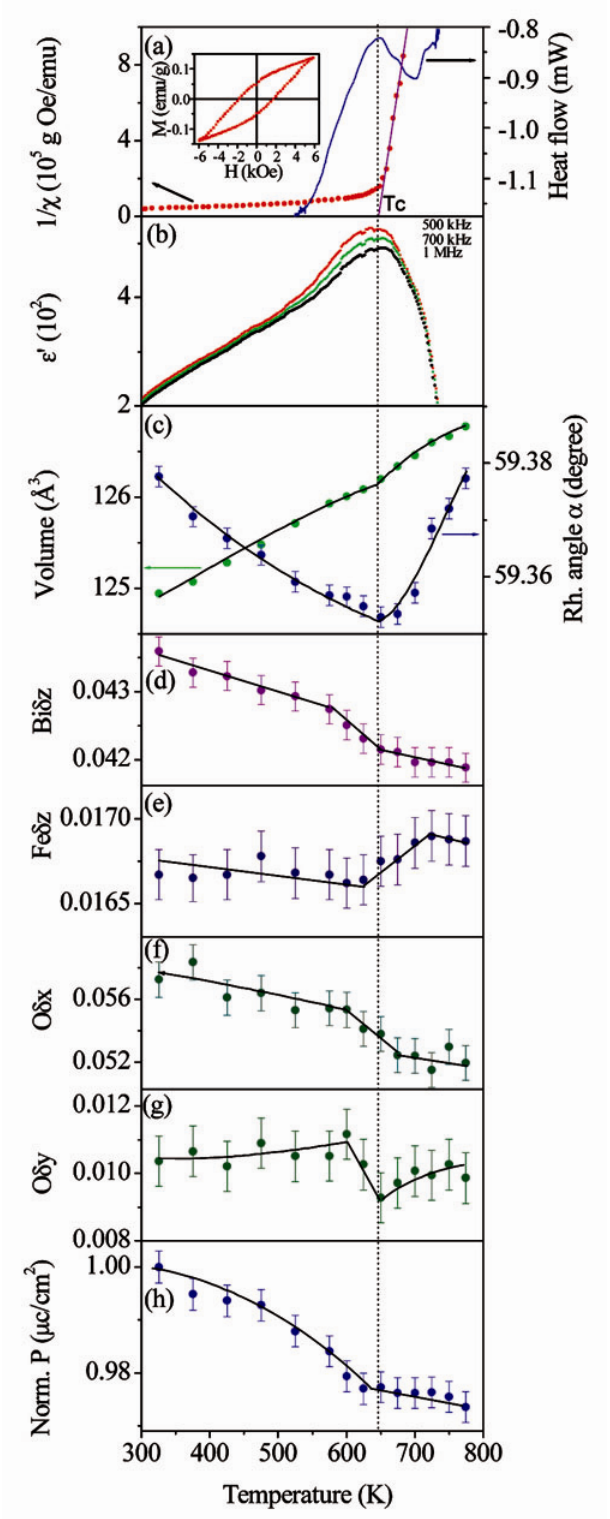

Figure 3. Temperature dependence of (a) inverse of the magnetic susceptibility (dotted line) measured at 500 Oe and background subtracted heat flow (continuous line), (b) the real part of the dielectric constant at various selected frequencies, (c) rhombohedral distortion angle and the unit cell volume, change in atomic coordinates of Bi_z (d), Fe_z (e), O_x (f) and O_y (g) from their ideal positions and (h) polarization calculated using simple ionic model. The inset to figure (a) depicts the *M*–*H* hysteresis loop at 300 K (after Singh *et al* 2008).

transition is unusual as there is no change of space group. We thus conclude that the shift of the atomic positions below the magnetic transition temperature is due to an isostructural phase transition. The isostructural phase transition, though very rare, has been reported in another multiferroic $LuMnO_3$ (Lee *et al* 2008a) but at very low temperatures.

We have calculated the polarization of BF–0·1BT at various temperatures using a simple ionic model expression, $Ps = (1/V)\Sigma q_i r_i$, where q_i, is the nominal charge of ith atom, r_i its atomic position in the unit cell and V the volume of the primitive unit cell, and the sum runs over all the atoms inside the unit cell. We present our calculated electric polarization P along $[111]_R$ in figure 3(h) after normalizing them with respect to the value obtained at 325 K. The large shift in the Bi position in the magnetic phase leads to a jump in the polarization in the magnetic phase. The excess polarization in the magnetic phase scales nearly linearly with the magnetization, as shown in figure 6 confirming linear magnetoelectric coupling in BF–0·1BT. Our results provide the first direct atomic level evidence for magnetoelectric coupling of

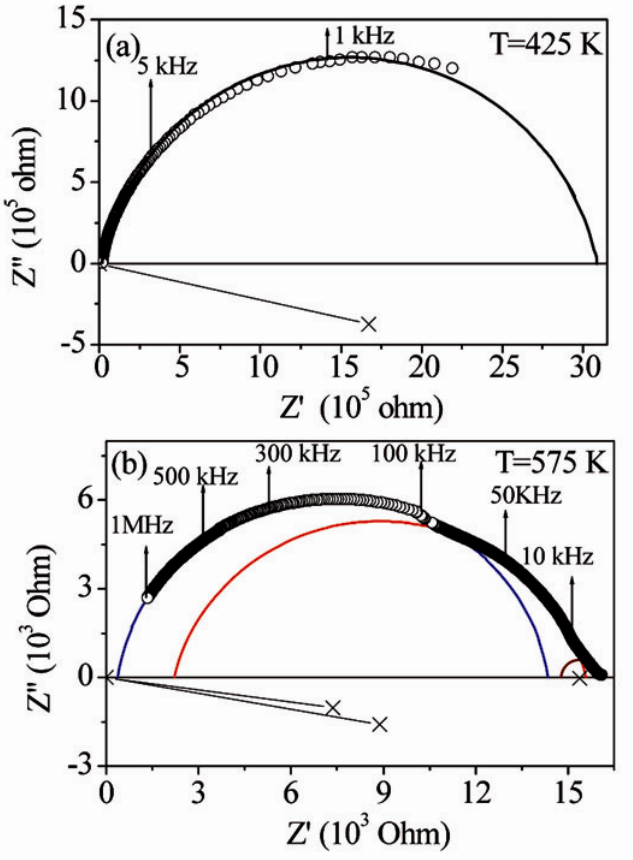

Figure 4. Cole–Cole plots of complex-impedance (Z'' vs Z') at (a) 425 K and (b) 575 K. Symbols are experimental data in the frequency range 100 Hz to 1 MHz, while the semicircular arcs are the fitted depressed circles (after Singh *et al* 2008).

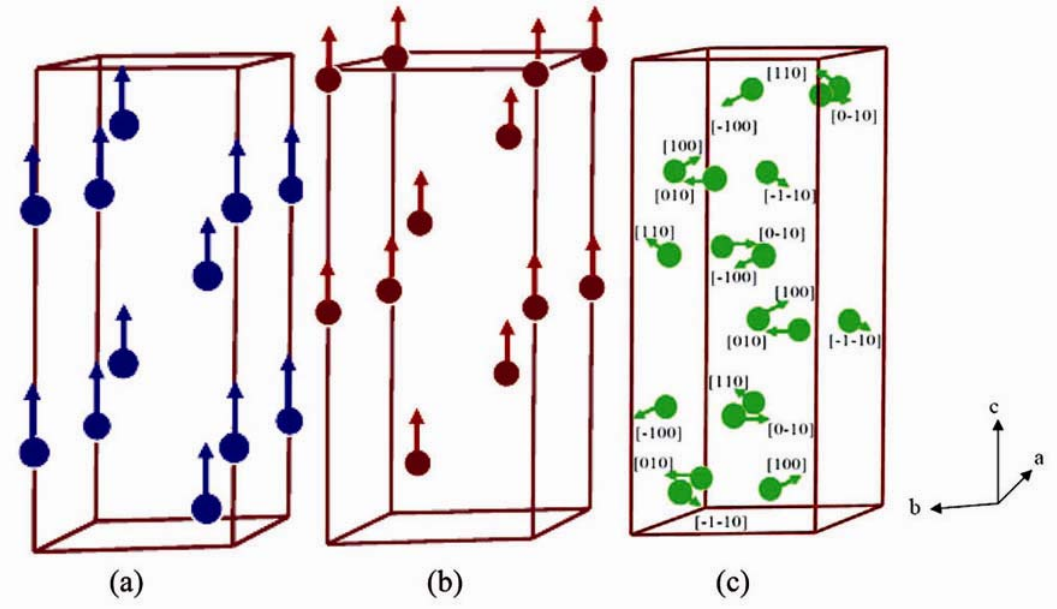

Figure 5. Theoretical displacement of (a) Bi^{3+}/Ba^{2+}, (b) Fe^{3+}/Ti^{4+} and (c) O^{2-} (after EPAPS Document 2008).

Table 3. Theoretical calculation of basis function of irreducible representation with displacement vectors for the symmetry $R3c$ with $k = 0$ for the Wyckoff site 18*b*: O (1/6 – 2*e* – 2*d*, 1/3 – 4*d*, 1/12) (after EPAPS Document 2008).

			Site 18*b*					
Irred. reps.	Basis function		(x, y, z)	$(-y+1, x-y+1, z)$	$(-x+y, -x+1, z)$	$(-y+1/3, -x+2/3, z+1/6)$	$(-x+y, y, z+1/2)$	$(x, x-y+1, z+1/2)$
IR(1)	Basis (1)		(100)	(010)	(–1 –10)	(0 –10)	(–100)	(110)
	Basis (2)		(010)	(–1 –10)	(100)	(–100)	(110)	(0 –10)
	Basis (3)		(001)	(001)	(001)	(001)	(001)	(001)
IR(2)	Basis (1)		(100)	(010)	(–1 –10)	(010)	(100)	(–1 –10)
	Basis (2)		(010)	(–1 –10)	(100)	(100)	(–1 –10)	(010)
	Basis (3)		(001)	(001)	(001)	(00 –1)	(00 –1)	(00 –1)
IR(3)	Basis (1)	Re	(1·00 0·00 0·00)	(0·00 –0·50 0·00)	(0·50 0·50 0·00)	(0·00 0·00 0·00)	(0·00 0·00 0·00)	(0·00 0·00 0·00)
		Im	0·00 0·00 0·00)	(0·00 –0·87 0·00)	(–0·87 –0·87 0·00)	(0·00 0·00 0·00)	(0·00 0·00 0·00)	(0·00 0·00 0·00)
	Basis (2)	Re	(0·00 1·00 0·00)	(0·50 0·50 0·00)	(–0·50 0·00 0·00)	(0·00 0·00 0·00)	(0·00 0·00 0·00)	(0·00 0·00 0·00)
		Im	(0·00 0·00 0·00)	(0·87 0·87 0·00)	(0·87 0·00 0·00)	(0·00 0·00 0·00)	(0·00 0·00 0·00)	(0·00 0·00 0·00)
	Basis (3)	Re	(0·00 0·00 1·00)	(0·00 0·00 –0·50)	(0·00 0·00 –0·50)	(0·00 0·00 0·00)	(0·00 0·00 0·00)	(0·00 0·00 0·00)
		Im	(0·00 0·00 0·00)	(0·00 0·00 –0·87)	(0·00 0·00 0·87)	(0·00 0·00 0·00)	(0·00 0·00 0·00)	(0·00 0·00 0·00)
	Basis (4)	Re	(0·00 0·00 0·00)	(0·00 0·00 0·00)	(0·00 0·00 0·00)	(0·00 –1·00 0·00)	(0·50 0·00 0·00)	(–0·50 –0·50 0·00)
		Im	(0·00 0·00 0·00)	(0·00 0·00 0·00)	(0·00 0·00 0·00)	(0·00 0·00 0·00)	(–0·87 0·00 0·00)	(–0·87 –0·87 0·00)
	Basis (5)	Re	(0·00 0·00 0·00)	(0·00 0·00 0·00)	(0·00 0·00 0·00)	(–1·00 0·00 0·00)	(–0·50 –0·50 0·00)	(0·00 0·50 0·00)
		Im	(0·00 0·00 0·00)	(0·00 0·00 0·00)	(0·00 0·00 0·00)	(0·00 0·00 0·00)	(0·87 0·87 0·00)	(0·00 0·87 0·00)
	Basis (6)	Re	(0·00 0·00 0·00)	(0·00 0·00 0·00)	(0·00 0·00 0·00)	(0·00 0·00 1·00)	(0·00 0·00 –0·50)	(0·00 0·00 –0·50)
		Im	(0·00 0·00 0·00)	(0·00 0·00 0·00)	(0·00 0·00 0·00)	(0·00 0·00 0·00)	(0·00 0·00 0·87)	(0·00 0·00 –0·87)
	Basis (7)	Re	(0·00 0·00 0·00)	(0·00 0·00 0·00)	(0·00 0·00 0·00)	(0·00 –1·00 0·00)	(0·50 0·00 0·00)	(–0·50 –0·50 0·00)
		Im	(0·00 0·00 0·00)	(0·00 0·00 0·00)	(0·00 0·00 0·00)	(0·00 0·00 0·00)	(0·87 0·00 0·00)	(0·87 0·87 0·00)
	Basis (8)	Re	(0·00 0·00 0·00)	(0·00 0·00 0·00)	(0·00 0·00 0·00)	(–1·00 0·00 0·00)	(–0·50 –0·50 0·00)	(0·00 0·50 0·00)
		Im	(0·00 0·00 0·00)	(0·00 0·00 0·00)	(0·00 0·00 0·00)	(0·00 0·00 0·00)	(–0·87 –0·87 0·00)	(0·00 –0·87 0·00)
	Basis (9)	Re	(0·00 0·00 0·00)	(0·00 0·00 0·00)	(0·00 0·00 0·00)	(0·00 0·00 1·00)	(0·00 0·00 –0·50)	(0·00 0·00 –0·50)
		Im	(0·00 0·00 0·00)	(0·00 0·00 0·00)	(0·00 0·00 0·00)	(0·00 0·00 0·00)	(0·00 0·00 –0·87)	(0·00 0·00 0·87)
	Basis (10)	Re	(1·00 0·00 0·00)	(0·00 –0·50 0·00)	(0·50 0·50 0·00)	(0·00 0·00 0·00)	(0·00 0·00 0·00)	(0·00 0·00 0·00)
		Im	(0·00 0·00 0·00)	(0·00 0·87 0·00)	(0·87 0·87 0·00)	(0·00 0·00 0·00)	(0·00 0·00 0·00)	(0·00 0·00 0·00)
	Basis (11)	Re	(0·00 1·00 0·00)	(0·50 0·50 0·00)	(–0·50 0·00 0·00)	(0·00 0·00 0·00)	(0·00 0·00 0·00)	(0·00 0·00 0·00)
		Im	(0·00 0·00 0·00)	(–0·87 –0·87 0·00)	(–0·87 0·00 0·00)	(0·00 0·00 0·00)	(0·00 0·00 0·00)	(0·00 0·00 0·00)
	Basis (12)	Re	(0·00 0·00 1·00)	(0·00 0·00 –0·50)	(0·00 0·00 –0·50)	(0·00 0·00 0·00)	(0·00 0·00 0·00)	(0·00 0·00 0·00)
		Im	(0·00 0·00 0·00)	(0·00 0·00 0·87)	(0·00 0·00 –0·87)	(0·00 0·00 0·00)	(0·00 0·00 0·00)	(0·00 0·00 0·00)

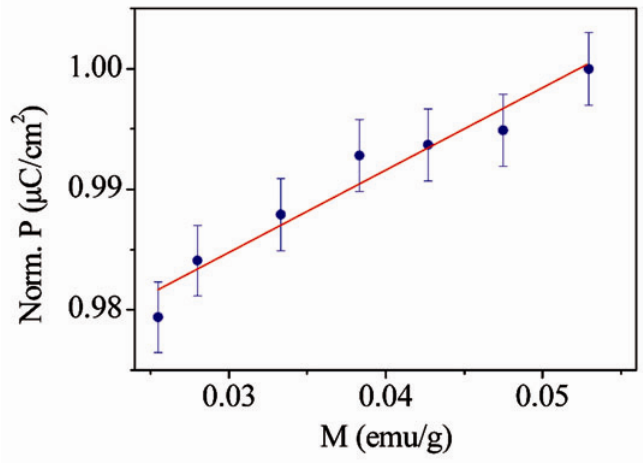

Figure 6. Variation of the polarization with magnetization (after Singh *et al* 2008).

intrinsic multiferroic origin in a $BiFeO_3$ based compositions. A similar study on the $(1-x)BiFeO_3$–$xPbTiO_3$ system has also revealed magnetoelectric coupling of intrinsic multiferroic origin (Bhattacharjee *et al* 2009; Bhattacharjee and Pandey, to be published).

We believe that the occurrence of isostructural phase transition accompanying the magnetic transition in multiferroics is a general feature of most multiferroics reflecting magnetoelectric coupling via magnetoelastic coupling. We also believe that our findings will encourage a systematic search for such a transition in other multiferroics as well.

Acknowledgement

One of the authors (AS) acknowledges support from UGC, India.

References

Aken B B V, Palstra T T M, Filippetti A and Spaldin N A 2004 *Nature Mater.* **3** 164
Bhattacharjee S and Pandey D, to be published
Bhattacharjee S, Tripathi S and Pandey D 2007 *Appl. Phys. Lett.* **91** 042903
Bhattacharjee S, Pandey V, Kotnala R K and Pandey D 2009 *Appl. Phys. Lett.* **94** 012906
Brink J V D and Khomskii D I 2008 *J. Phys.: Condens. Matter* **20** 434217
Catalan G 2006 *Appl. Phys. Lett.* **88** 102902
Cheong S W and Mostovoy M 2007 *Nature Mater.* **6** 13
Eerenstein W, Morrisonet F D, Dho J, Blamire M G, Scott J F and Mathur N D 2005 *Science* **307** 1203a
Eerenstein W, Mathur N D and Scott J F 2006 *Nature* **442** 759
EPAPS Document 2008 No. E-PRLTAO-101-092849 (http://www.aip.org/pubservs/epaps.html)
Fiebig M 2005 *J. Phys.* **D38** R123
Fischer P, Polomska M, Sosnowska I and Szymanski M 1980 *J. Phys. C: Solid State Phys.* **13** 1931
Glazer A M 1972 *Acta Crystallogr.* **B28** 3384
Hill N A 2000 *J. Phys. Chem.* **B104** 6694
Hovestreydt E, Aroyo M, Sattler S and Wondratschek H 1992 *J. Appl. Cryst.* **25** 544
Jacobson A J and Fender B E F 1975 *J. Phys. C. Solid State Phys.* **8** 844
Kimura T, Goto T, Shintani H, Ishizaka K, Arima T and Tokura Y 2003a *Nature* **426** 55
Kimura T, Kawamoto S, Yamada I, Azuma M, Takano M and Tokura Y 2003b *Phys. Rev.* **B67** 180401
Kumar M M and Palkar V R 2000 *Appl. Phys. Lett.* **76** 2764
Lebeugle D, Colson D, Forget A and Viret M 2007 *Appl. Phys. Lett.* **91** 022907
Lebeugle D, Colson D, Forget A, Viret M, Bataille A M and Gukasov A 2008 *Phys. Rev. Lett.* **100** 227602
Lee S *et al* 2008a *Nature* **451** 805
Lee S, Ratcliff W, Cheong S W and Kiryukhin V 2008b *Appl. Phys. Lett.* **92** 192906
Mazumder R, Devi P S, Bhattacharya D, Choudhury P and Sen A 2007 *Appl. Phys. Lett.* **91** 062510
Megaw H D and Darlington C N W 1975 *Acta Crystallogr.* **A31** 161
Palewicz A, Przniosto R, Sosnowska I and Hewat A W 2007 *Acta Crystallogr.* **B63** 537
Popov Y F, Zvezdin A K, Vorobev G P, Kadomtseva A M, Murashev V A and Rokov D N 1993 *JETP Lett.* **57** 169
Ramesh R and Spaldin N A 2007 *Nature Mater.* **6** 21
Rao C N R and Serrao C R 2007 *J. Mater. Chem.* **17** 4931
Ruette B, Zvyagin S, Pyatakov A P, Bush A, Li J F, Belotelov V I, Zvezdin A K and Viehland D 2004 *Phys. Rev.* **B69** 064114
Singh A, Pandey V, Kotnala R K and Pandey D 2008 *Phys. Rev. Lett.* **101** 247602
Sosnowska I, Neumaier T P and Steichele E 1982 *J. Phys. C: Solid State Phys.* **15** 4835
Wang J *et al* 2003 *Science* **299** 1719
Wang Y P, Zhou L, Zhang M F, Chen X Y, Liu J M and Liu Z G 2004 *Appl. Phys. Lett.* **84** 1731
Wang N, Cheng J, Pyatakov A, Zvezdin A K, Li J F, Cross L E and Viehland D 2005 *Phys. Rev.* **B72** 104434
Zhang S T, Lu M H, Wu D, Chen Y F and Ming N B 2005 *Appl. Phys. Lett.* **87** 262907